Effect of Geometrical Disturbance on Vortex Asymmetry

David Degani*
NASA Ames Research Center, Moffett Field, California 94035

The phenomena of the flow about a slender body of revolution placed at incidence to an oncoming stream were numerically investigated for angles of attack of 20 and 40 deg and a Reynolds number of 2×10^5 based on maximum body diameter. At angle of attack of 20 deg, the flow was steady and symmetric, and the presence of a perturbation, which was placed near the tip of the body, made only a small change. At angle of attack of 40 deg, the flow was found to be steady (except for a small-amplitude, high-frequency unsteadiness of the shear layer), but became highly asymmetric when a space-fixed, time-invariant disturbance was added near the tip. The level of the asymmetry was dependent on the size and location of the disturbance. When the disturbance was removed, the flowfield relaxed to its original symmetric shape. On the basis of this observation, experimental data, and other theoretical indicators, it is suggested that the origin of the asymmetry is a convective-type instability of the originally symmetric flow.

Nomenclature

a_∞ = speed of sound
C_N = normal-force coefficient
C_p = pressure coefficient
C_Y = side-force coefficient
D = maximum diameter of body
h = disturbance height
M_∞ = freestream Mach number
Re_D = Reynolds number based on D
$\tilde{t}$ = nondimensional time, $= ta_\infty/D$
x,y,z = coordinate system
α = angle of attack
ρ = density
ϕ = circumferential roll angle

Introduction

THE flow observed about a slender body of revolution placed at incidence to an oncoming stream exhibits a wide variety of phenomena.[1-4] As the angle of attack is increased from zero, a steady, symmetric pair of vortices is observed in the leeward-side flow. With further increase in incidence, the symmetric vortex pair becomes asymmetric, but the flow remains steady in time. At still higher incidence, the steady asymmetric flow evolves to a steady pattern of multiple vortices that leave from alternate sides of the body with increasing distance downstream. With further increase in incidence, the asymmetric flow becomes nonsteady, and as the angle of attack tends toward 90 deg, the flow pattern approaches that of a circular cylinder in crossflow (except for the region near the nose). It is well known that at low Reynolds numbers flow about the cylinder is steady and symmetric. However, when the Reynolds number is increased beyond a critical value ($Re_D \approx 50$) the flow becomes nonsteady. Vortices are shed periodically from alternate sides of the cylinder and are convected downstream to form the classic Karman vortex street.

Received Nov. 20, 1989; presented as Paper 90-0593 at the AIAA 28th Aerospace Sciences Meeting, Reno, NV, Jan. 8-11, 1990; revision received March 20, 1990; accepted for publication April 12, 1990.

*National Research Council Senior Research Associate; Associate Professor, Technion—Israel Institute of Technology, Faculty of Mechanical Engineering. Associate Fellow AIAA.

Time-accurate computations of two-dimensional flow about a circular cylinder[5-7] (using algorithms that are unbiased in the circumferential direction) have revealed that, unless a symmetry-breaking perturbation was introduced into the flow, the solutions remained symmetric and steady. The perturbations were typically introduced for a short period of time, then removed, and the flows advanced in time until the oscillatory solution was developed.

The mechanisms that lead to an asymmetric vortex wake in three-dimensional flow are not well understood at the present time. Several mechanisms for laminar and fully turbulent flows[8,9] and for transitional flows[10] have been advanced. First, it has been suggested that the asymmetry is a result of an instability of the flow in the crossflow planes above the body. Second, it has been suggested that the asymmetry occurs due to an asymmetric transition of the boundary-layer flow.

In Refs. 11-13, Degani and Schiff utilized a time-accurate thin-layer Navier-Stokes code[14] to study the three-dimensional, subsonic laminar flow surrounding a slender body of revolution at large incidence. Computed results for the flow surrounding an ogive cylinder at $M_\infty = 0.2$, $\alpha = 40$ deg, and Reynolds number $= 2 \times 10^5$ (based on freestream conditions and cylinder diameter) indicated that the computed flow remained symmetric at angles of attack where experimental measurements showed the presence of large asymmetry. Guided by the results for the two-dimensional cylinder flow, the authors applied a transient symmetry-breaking perturba-

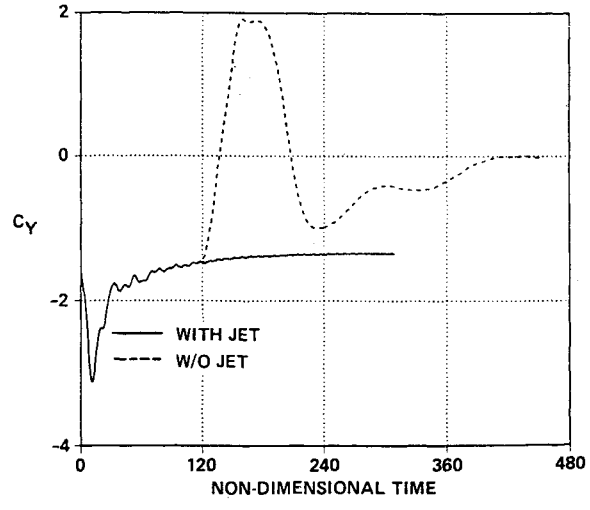

Fig. 1 Side-force coefficient history: $M_\infty = 0.2$, $\alpha = 40$ deg, $Re_D = 2.6 \times 10^4$ (Ref. 13).

tion to induce asymmetry. When the perturbation (a small surface jet blowing normal to the surface and perpendicular to the angle-of-attack plane) was introduced, the solution started to evolve to an asymmetric state. If the jet was kept on at constant strength, the computed flow reached and maintained an asymmetric state. However, in contrast to the results of the computations for two-dimensional vortex shedding, when the jet was turned off,[13] the asymmetry in the flow began to dissipate and the flow returned to a symmetric state, as demonstrated in Fig. 1.

In the current work, Navier-Stokes computations have been applied to further investigate the phenomena governing the onset of vortex asymmetry. To simulate more realistically the body surface boundary conditions, the jet that was used previously was replaced by a small geometrical disturbance. Time-accurate solutions were obtained for flow over an ogive-cylinder body for angles of attack of $\alpha = 20$ and 40 deg and a Reynolds number $= 2 \times 10^5$ (based on freestream conditions and cylinder diameter).

Theoretical Background

Governing Equations

The conservation equations of mass, momentum, and energy can be represented in a flux-vector form that is convenient for numerical simulation as[15]

$$\partial_\tau \hat{Q} + \partial_\xi (\hat{F} + \hat{F}_v) + \partial_\eta (\hat{G} + \hat{G}_v) + \partial_\zeta (\hat{H} + \hat{H}_v) = 0 \qquad (1)$$

where τ is the time and the independent spatial variables ξ, η, and ζ are chosen to map a curvilinear body-conforming grid into a uniform computational space. In Eq. (1), $\hat{Q}$ is the vector of dependent flow variables; $\hat{F} = \hat{F}(\hat{Q})$, $\hat{G} = \hat{G}(\hat{Q})$, and $\hat{H} = \hat{H}(\hat{Q})$ are the inviscid flux vectors; and the terms $\hat{F}_v$, $\hat{G}_v$, and $\hat{H}_v$ are fluxes containing derivatives of the viscous terms. A nondimensional form of the equations is used throughout this work. The conservative form of the equations is maintained chiefly to capture shock waves in transonic and supersonic flows as accurately as possible.

Several numerical investigations of two-dimensional unsteady separated flows,[34] three-dimensional steady flows over slender bodies having crossflow separation,[35] and, more recently, three-dimensional flows over a supersonic delta wing[36] showed insignificant differences between full Navier-Stokes calculations and the thin-layer approximation. On the other hand, the thin-layer approximation can save up to 15% of the CPU time of the calculations and, therefore, the thin-layer

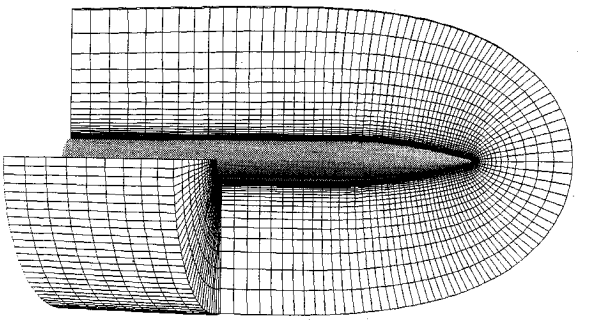

Fig. 2 Tangent ogive-cylinder grid.

approximation was used in the present calculations. For body-conforming coordinates where ζ is the coordinate leading away from the surface, the thin-layer approximation yields[16,17]

$$\partial_\tau \hat{Q} + \partial_\xi \hat{F} + \partial_\eta \hat{G} + \partial_\zeta \hat{H} = Re^{-1} \partial_\zeta \hat{S} \qquad (2)$$

where only viscous terms in ζ are retained. These have been collected into the vector $\hat{S}$ and the nondimensional Reynolds number Re is factored from the viscous flux term. The coefficients of viscosity and thermal conductivity that appear in Eq. (2) are specified from auxiliary relations. The coefficient of laminar viscosity is obtained using Sutherland's law. The coefficient of thermal conductivity is obtained once the viscosity coefficient is known by assuming a constant Prandtl number.

The implicit scheme employed in this study is the algorithm reported by Steger et al.[14] The algorithm uses flux-vector splitting [18] and upwind spatial differencing for the convection terms in one coordinate direction (nominally streamwise).

The finite difference scheme uses flux splitting in the ξ direction and central differencing in the η and ζ directions. As a consequence, numerical dissipation terms denoted by Di and De in Eq. (49) are employed in the η and ζ directions and are given as combinations of second and fourth differences. The second-order smoothing terms act to control numerical oscillations across shock waves, whereas the fourth-order smoothing is effective elsewhere. In order to improve the accuracy of the solutions, the fourth-order numerical smoothing terms are further scaled by q/q_∞. This has the effect of reducing the numerical smoothing in the viscous layer adjoining the body surface where viscous dissipation controls the dispersion, and where additional numerical smoothing terms can adversely affect the accuracy of the solution by modifying the physical viscous terms.

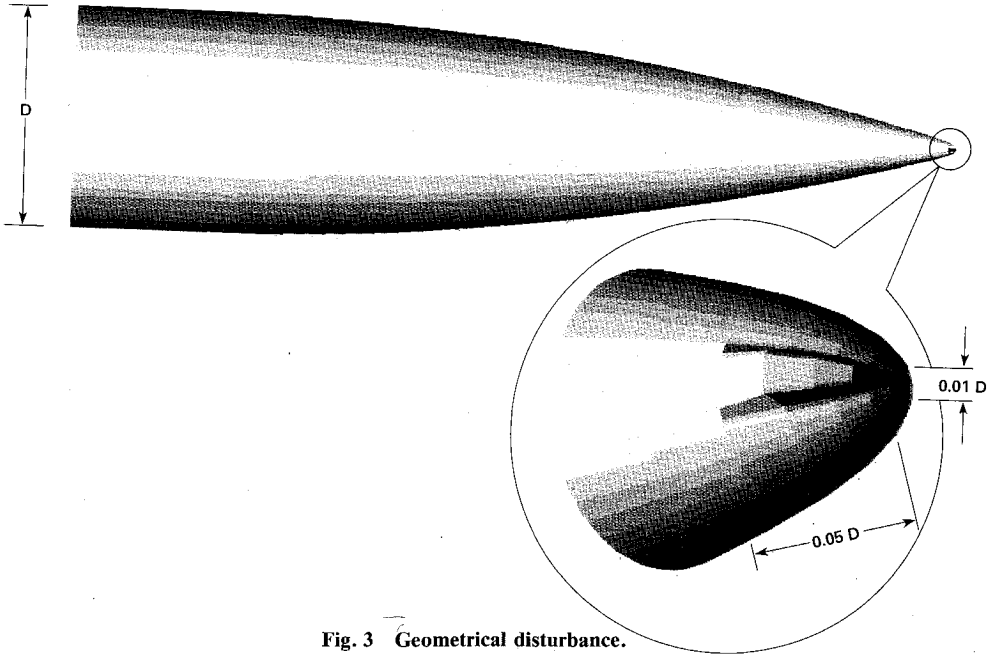

Fig. 3 Geometrical disturbance.

Body Configurations and Computational Grids

Computations were performed for subsonic flow over an ogive-cylinder body, which consisted of 3.5-diam tangent ogive forebody with a 7.0-diam cylindrical afterbody extending aft of the nose-body junction to $x/D = 10.5$.

The grid consisted of 120 equispaced circumferential planes ($\Delta\phi = 3$ deg) extending completely around the body. In each circumferential plane, the grid contained 50 radial points between the body surface and the computational outer boundary and 59 axial points between the nose and the rear of the body (Fig. 2). This grid spacing was found adequate for similar flowfields in previous calculations.[11-13]

Boundary Conditions and Initial Conditions

An adiabatic no-slip boundary condition was applied at the body surface, and undisturbed freestream conditions were maintained at the computational outer boundary. An implicit periodic continuation condition was imposed at the circumferential edges of the grid, and at the downstream boundary, a simple zero-axial-gradient extrapolation condition was applied. This simple extrapolation boundary condition is not strictly valid in subsonic flow because the body wake can affect the flow on the body. However, by letting the computed body length extend beyond the physical length of the experimental model[3,4] and by neglecting the portion of the flow near the downstream boundary, the effect of the boundary can be minimized. On the upstream axis of symmetry an extrapolation boundary condition was used to obtain the flow conditions on the axis from the cone of points one axial plane downstream.

In these computations, a time-accurate solution was required. Thus, the second-order, time-accurate algorithm was used with a globally constant time step. The flowfield was initially set to freestream conditions throughout the grid, or to a previously obtained solution, and the flowfield was advanced in time until a solution was obtained.

A small geometrical bump was added to the body surface to act as a symmetry-breaking perturbation (Fig. 3). The height of the bump ranged from 0.005 to 0.02 of the body diameter, the length of the bump was 0.05 of the body diameter and it was located at $x/D \approx 0.025$ and 90 deg circumferentially from the windward meridian.

The code required approximately 8×10^{-5} s/iteration/grid point on the NAS CRAY-2 computer. This translates to approximately 27 s/iteration. Further, the need to resolve the thin viscous layers for high Reynolds number flow required that the grid have a fine radial spacing at the body surface. As a result, the allowable computational nondimensional time steps were found to range from 0.008 to 0.010.

Results

$\alpha = 20$ Deg

At a low angle of attack, $\alpha = 20$ deg, the flow as observed experimentally[3,4,9,19,20] is almost symmetric. Results of previous computations[11-13,21] for this angle of attack were perfectly symmetric and agreed very well with experimental results.[9] To test the effect of roughness at low angles of attack, a small geometrical perturbation was introduced, as explained earlier, with $h/D = 0.02$. Although the size of the perturbation in this case is not negligible (twice the size of the maximum perturbation that was used for other cases), the change in the flow is small. This is demonstrated in Figs. 4, which present computed circumferential surface pressure coefficient distributions against experimental data[9] for three axial locations. It can be seen from Figs. 4 that the agreement between the computed and measured pressures is very good for all stations. Figure 5 shows the effect of the perturbation on the side-force coefficient as a function of time. The maximum value of the side-force coefficient is less than 5% of the normal force coefficient. The vortical flowfield above the body has very little asymmetry, as can be seen in Figs. 6. Figure 6a shows the

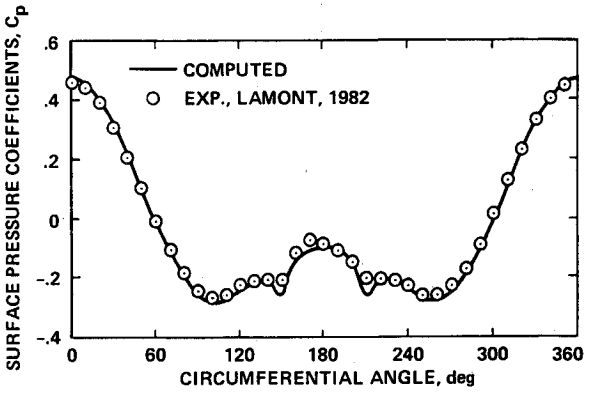

a) $x/D = 0.5$

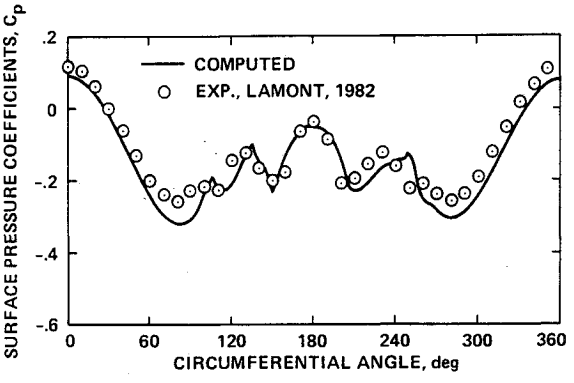

b) $x/D = 3.5$

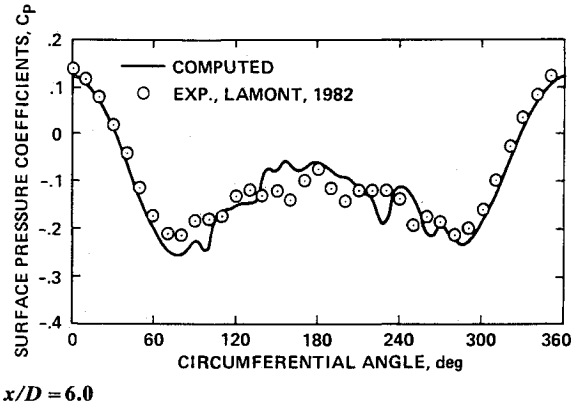

c) $x/D = 6.0$

Fig. 4 Circumferential surface pressure distributions: $h/D = 0.02$, $M_\infty = 0.2$, $\alpha = 20$ deg, $Re_D = 2 \times 10^5$.

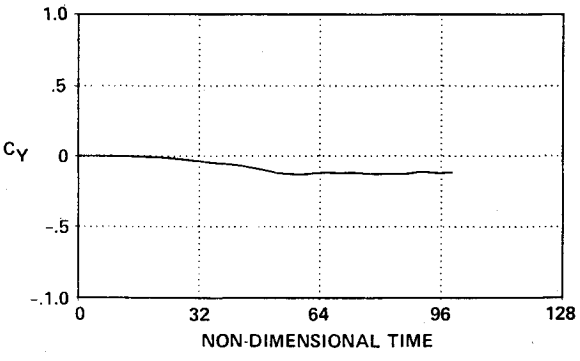

Fig. 5 Side-force coefficient history: $h/D = 0.02$, $M_\infty = 0.2$, $\alpha = 20$ deg, $Re_D = 2 \times 10^5$.

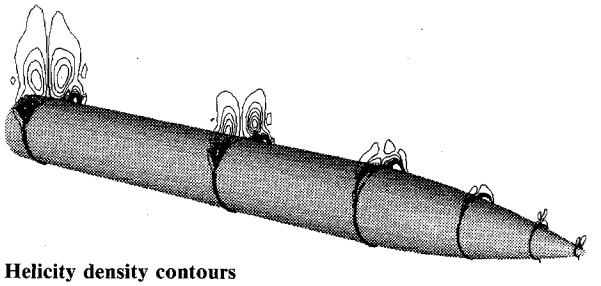

a) Helicity density contours

b) Off-surface streamlines

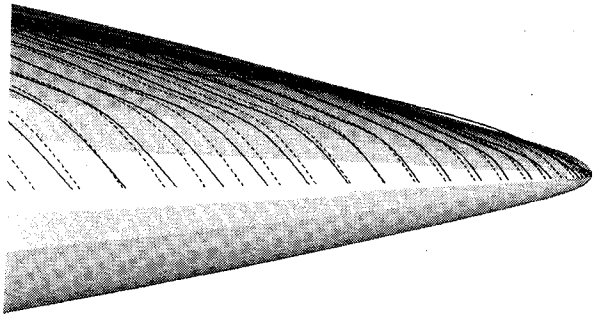

c) Enlargement of the flowfield near the tip

Fig. 6 Computational results (with geometrical disturbance) for $h/D = 0.02$, $M_\infty = 0.2$, $\alpha = 20$ deg, $Re_D = 2 \times 10^5$, $\tilde{t} = 97$.

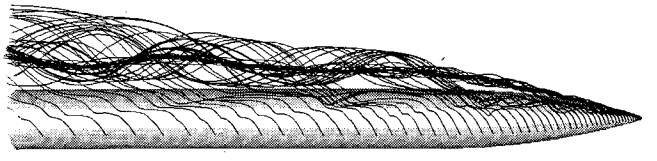

Fig. 7 Off-surface streamlines—symmetric case: $\alpha = 40$ deg, $M_\infty = 0.2$, $Re_D = 2 \times 10^5$, $\tilde{t} = 120$.

computed helicity density contours in several cross sections along the body. (Helicity density is defined as the scalar product of the local velocity and vorticity vectors. Since it indicates both the strength and sense of rotation of the vortices, helicity density has been found to be an excellent means of visualizing the position and strength of the vortex pattern.[22,23] By marking positive and negative values of helicity with different colors it is easy to differentiate between the primary and secondary vortices.) Only small differences can be observed between the two primary vortices on both sides of the body. The corresponding off-surface streamline pattern (Fig. 6b) shows the presence of a pair of almost symmetric primary vortices. The vortices are almost parallel and close to the upper body surface. The change of the streamline pattern between both sides of the body is very moderate. This can be seen more clearly from the enlargement in Fig. 6c of the flowfield near the tip, which does not show a significant distortion of the almost symmetric flowfield (the dashed lines represent streamlines on the far side of the body).

$\alpha = 40$ Deg

Previous computations[11-13] showed that even for an angle of attack of 40 deg the computed flow remains symmetric and is stable to small, temporal perturbations. Figure 7 shows the off-surface streamline pattern for this symmetric case. The two vortices that originate at the nose run almost parallel to the body upper surface as they grow with distance downstream. In contrast to experimental observations,[3,4,19,20,24] the computed vortices do not appear to curve away from the body surface.

It has been suggested already (cf., e.g., Refs. 12, 13, 19, 20, 24) that vortex asymmetry originates from imperfections of the nose. It was also demonstrated [12,13] that it is essential to introduce a space-fixed, time-invariant perturbation (a small jet in Refs. 12 and 13) into the computation to simulate the imperfection. In the current work, to simulate the physics more realistically, rather than using a jet, a geometrical perturbation was added to the body at $x/D \approx 0.025$ and with maximum height of $h/D = 0.01$ (Fig. 3). Figures 8 demonstrate the dramatic change in the flowfield that resulted from the perturbation. The flowfield became highly asymmetric, as shown in the helicity density contours in Fig. 8a. The corre-

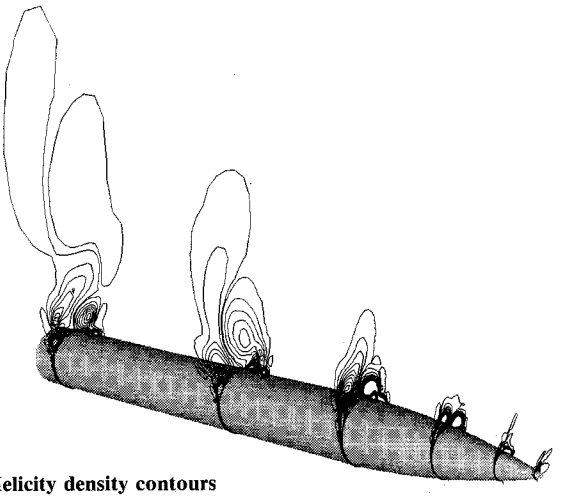

a) Helicity density contours

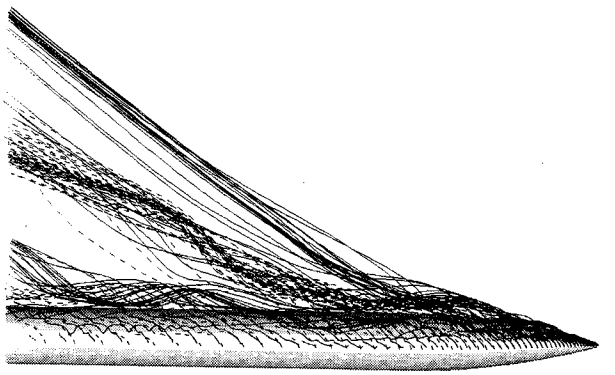

b) Off-surface streamlines

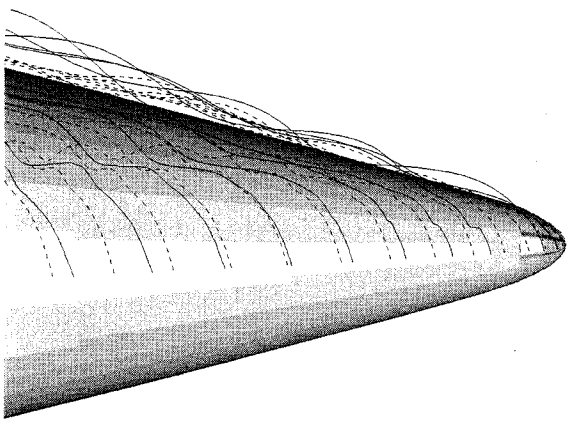

c) Enlargement of the flowfield near the tip

Fig. 8 Computational results (with geometrical disturbance) for $h/D = 0.01$, $\alpha = 40$ deg, $M_\infty = 0.2$, $Re_D = 2 \times 10^5$, $\tilde{t} = 235$.

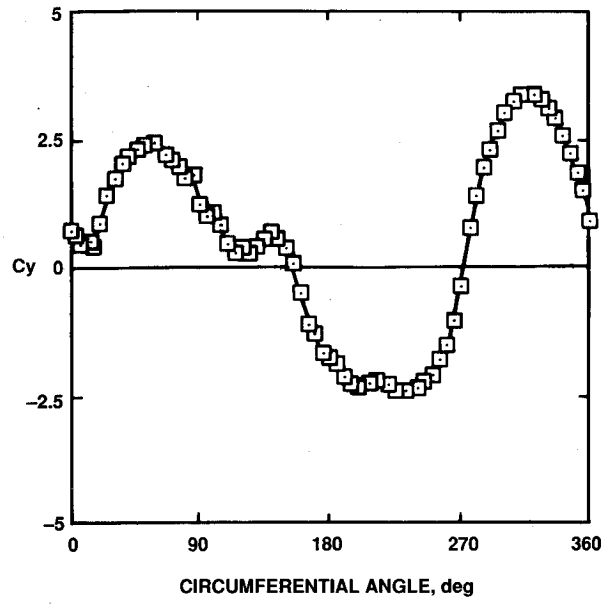

Fig. 9 Side-force coefficient vs nose roll angle (Ref. 25): $\alpha = 40$ deg, $Re_D = 3 \times 10^4$.

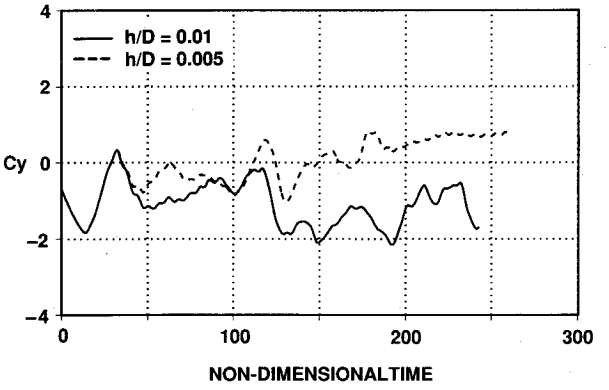

Fig. 10 Side-force coefficient history: $\alpha = 40$ deg, $M_\infty = 0.2$, $Re_D = 2 \times 10^5$.

sponding off-surface streamline pattern (Fig. 8b) shows the presence of two pairs of primary vortices. The upstream pair is highly asymmetric and the vortices curve away from the body surface about one and a half body diameters from the tip. Upstream of the point when the vortices lift off, the change of the streamline pattern between both sides of the body is very moderate (the dashed lines represent streamlines on the far side of the body). This can be seen more clearly from the enlargement of the flowfield near the tip (Fig. 8c) and also by comparing Fig. 8b to Fig. 7. The flow asymmetry in the vicinity of the geometric disturbance is very small but grows nonlinearly beyond the point where the vortices lift off. Downstream, the vortices are not parallel to the freestream but are inclined approximately 5 deg toward the body from the freestream direction. The second pair of vortices run almost parallel to the body surface but they start to lift off near the aft end of the body. When the disturbance was removed, the flowfield relaxed back to a symmetric state, as was previously demonstrated for the jet in the earlier studies.[11-13]

It was found experimentally (cf. Refs. 3, 4, 9, 19, 20, 24, 25) that at angle of attack of about 40 deg, as the size or the location of the disturbance changed, the position of the first pair of primary vortices changed in what appeared to be an arbitrary way, sometimes even to the extent of becoming almost symmetric. Furthermore, these experiments show that the variation of side-force coefficients with nose roll angle (for a symmetric nose) is almost a sine wave, as can be seen in Fig. 9 (taken from Ref. 25). From this figure, it is obvious that the vortex pattern does not have any preferred orientation (and similar results were obtained by others). For higher angles of attack, 50–60 deg, the character of the variation with nose roll angle changes from continuous distribution to one approaching a square wave distribution.[25,33] The angle of attack in which the square wave distribution exists could be much lower if the tip geometry is disturbed.[25,33] It was also observed that for a given configuration there was a maximum extent of vortex asymmetry such that an increase in the level of the disturbance did not further increase the extent of asymmetry.[24]

In order to test the latter finding computationally, the size of the geometrical perturbation was cut to one half of the original size (i.e., $h/D = 0.005$). The computational results show a decrease in the extent of asymmetry and a change in sign of the total side-force coefficients, as shown in Figs. 10 and 11.

Figure 10 presents the time history of side-force coefficients for the last two cases, i.e., for $\alpha = 40$ deg, with two sizes of disturbances, $h/D = 0.01$ (solid line) and $h/D = 0.005$ (dashed line, which was started at a nondimensional time of $\tilde{t} = 32$). The side-force coefficients for the second case converge toward a positive value, whereas in the case of $h/D = 0.01$, the side-force coefficients fluctuate around a negative mean value. These values are within the range shown in Fig. 9 and in other experiments.[9,19,20,25] Figure 11 shows the off-surface streamline pattern for the case of $h/D = 0.005$. In comparison to Fig. 8b, the first two primary vortices are positioned lower above the body upper surface and the asymmetry is smaller in extent. It is also evident that the vortex on the far side of the body (marked by dashed lines) is higher than the one on the near side (where the disturbance is located). This may explain why the side-force coefficients are positive for this case, whereas in the case of $h/D = 0.01$, the side-force coefficients are negative.

Discussion and Conclusions

The computational results presented in this paper and experimental findings (cf. Refs. 3,4,19,20,24,25) suggest that, at least over a certain range of Reynolds number, the trend of flowfields around slender bodies at incidence up to 50–60 deg can be roughly divided into two main groups (and the range of incidence for each group may change by ± 10 deg, depending on the quality of flow, body finish, etc.).

0 Deg < α < 30 Deg

In this range of angles of attack, the flow is steady and symmetric. At angles of attack above 10 deg (depending on flow conditions and the forebody shape), a pair of symmetric vortices appears and runs almost parallel to the body upper surface. Introduction of small disturbances near the tip (or at other locations along the body) has only a small effect on the symmetry of the flow and the flow relaxes back to its original state after the disturbances are removed.

30 Deg < α < 50 Deg

In this incidence range, the flow under normal conditions is usually asymmetric, but the level of the asymmetry depends on the amount of disturbances present on the tip of the body. It seems that the sensitivity of the flowfield increases as the disturbances are closer to the body apex, which suggests that

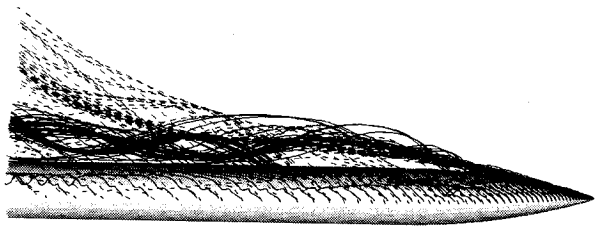

Fig. 11 Off-surface streamlines: $h/D = 0.005$, $M_\infty = 0.2$, $\alpha = 40$ deg, $Re_D = 2 \times 10^5$, $\tilde{t} = 235$.

the important parameter characterizing the effect of the disturbance is the ratio of the size of the disturbance to the local boundary-layer thickness. In other words, the effect of a small disturbance near the apex will be much larger in comparison to the case where the same disturbance is placed on the aft part of the body. It may also explain why the extent of the asymmetry is much smaller in the case of a blunt tip.[10,24] In this case, the thickness boundary layer at the tip is finite and large enough to reduce the effect of the natural disturbances, i.e., surface imperfections, etc. Since the tip in the present calculations is not a sharp one, but rather slightly rounded, it well may have a similar effect on the numerical results. (Preliminary results show that as the nose bluntness decreases the sensitivity of the flowfield to small disturbances increases.) The tip of a wind-tunnel model represents a large collection of disturbances, and, therefore, the final effect is the sum of the contributions of all disturbances. As a result, by changing the roll angle of the body, different patterns may evolve (and even an almost symmetric pattern of the vortices may appear[9,19,20,25,33]). Apparently, for laminar flows, the most sensitive circumferential angles to place a disturbance are between 90–140 deg from the windward plane of symmetry.[3,4,24] In the present calculations, perturbations were always placed at 90 deg.

Although the above mechanism gives a reasonable explanation for the behavior of the flowfield at this range of angles of attack, it fails in two main points. It does not explain why a small perturbation near the tip grows by several orders of magnitude as it convects downstream and it does not explain why the flowfield relaxes back to its original shape when the perturbation is removed (Fig. 1). The only mechanism that gives a satisfactory explanation to the whole is that of convective instability.

As mentioned earlier, the unsteady wake behind a two-dimensional cylinder is usually the result of an absolute instability, which means that any initial disturbance will grow in time and space. Because of nonlinear effects, the growth of the disturbance will reach an equilibrium state, and so the flow will evolve into a self-sustained oscillation of the wake (cf. Refs. 26–29). On the other hand, in the case of a convectively unstable wake (cf. Refs. 26, 29–31), all disturbances will be carried away, leaving finally the wake undisturbed, unless the disturbance is maintained for all time, (e.g., as in the case of the vibrating ribbon,[32] or as was done in the case of the flow over a rotating disk[30]). From the rapid growth of the disturbances in the wake of the ogive-cylinder body and from the fact that upon removal of the geometrical disturbance or the jet, the wake relaxed back to the initial symmetric flowfield, it is suggested that the asymmetric flow that exists for this range of angles of attack is the result of disturbing a convectively unstable symmetric flow. It is also worth mentioning that from the calculations and from experimental observations[3,4] the flow over the growing part of the body (i.e., the cone or the ogive forebody) is less asymmetric than that over the aft part of the body. This may explain why the experiments by Moskovitz et al.,[24] which presented pressures measured on the nose only, show, relative to other emperiments, smaller asymmetry for a given angle of attack. Also, the effect of unsteady vortex shedding could not be detected.

Acknowledgment

The author wishes to thank Murray Tobak and Lewis Schiff for helpful discussions.

References

[1]Hunt, B. L. "Asymmetric Vortex Wakes on Slender Bodies," AIAA Paper 82-1336, Aug. 1982.

[2]Ericsson, L. E., and Reding, J. P., "Aerodynamic Effects of Asymmetric Vortex Shedding from Slender Bodies," AIAA Paper 85-1797, Aug. 1985.

[3]Degani, D., and Zilliac, G. G., "Experimental Study of Unsteadiness of the Flow Around an Ogive-Cylinder at Incidence," AIAA Paper 88-4330, Aug. 1988.

[4]Degani, D., and Zilliac, G. G., "An Experimental Study of the Nonsteady Asymmetric Flow Around an Ogive-Cylinder at Incidence," *AIAA Journal*, Vol. 28, No. 4, 1990, pp. 642–649.

[5]Patel, V. A., "Karman Vortex Street behind a Circular Cylinder by the Series Truncation Method," *Journal of Computational Physics*, Vol. 28, 1978, pp. 14–42.

[6]Lecointe, Y., and Piquet, J., "On the Use of Several Compact Methods for the Study of Unsteady Incompressible Viscous Flow Round a Circular Cylinder," *Computers & Fluids*, Vol. 12, No. 4, 1984, pp. 255–280.

[7]Rosenfeld, M., Kwak, D., and Vinokur, M., "A Solution Method for the Unsteady and Incompressible Navier-Stokes Equations in Generalized Coordinate Systems," AIAA Paper 88-0718, Jan. 1988.

[8]Tobak, M., Chapman, G. T., and Unal, A., "Modeling Aerodynamic Discontinuities and Onset of Chaos in Flight Dynamical Systems," *Annale des Telecommunications*, Vol. 42, No. 5-6, 1987, pp. 300–314.

[9]Lamont, P.J., "Pressures Around an Inclined Ogive-Cylinder With Laminar, Transitional, or Turbulent Separation," *AIAA Journal*, Vol. 20, No. 11, 1982, pp. 1492–1499.

[10]Keener, E. R., and Chapman, G. T., "Similarity in Vortex Asymmetric Flows Over Slender Bodies and Wings," *AIAA Journal*, Vol. 15, No. 9, 1988, pp. 1370–1372.

[11]Degani, D., and Schiff, L. B., "Numerical Simulation of Asymmetric Vortex Flows Occurring on Bodies of Revolution at Large Incidence," AIAA Paper 87-2628, Aug. 1987.

[12]Degani, D., and Schiff, L. B., "Numerical Simulation of the Effect of Spatial Disturbances on Vortex Asymmetry," AIAA Paper 89-0340, Jan. 1989.

[13]Degani, D., and Schiff, L. B., "Numerical Simulation of the Effect of Spatial Disturbances on Vortex Asymmetry," *AIAA Journal* (to be published).

[14]Steger, J. L., Ying, S. X., and Schiff, L. B., "A Partially Flux-Split Algorithm for Numerical Simulation of Unsteady Viscous Flows," *Proceedings of a Workshop on Computational Fluid Dynamics*, Univ. of California, Davis, CA, 1986.

[15]Viviand, H., "Conservative Forms of Gas Dynamics Equations," *La Recherche Aerospatiale*, No. 1, 1974, pp. 65–68.

[16]Baldwin, B. S., and Lomax, H., "Thin Layer Approximation and Algebraic Model for Separated Turbulent Flows," AIAA Paper 78-257, Jan. 1978.

[17]Steger, J. L., "Implicit Finite-Difference Simulation of Flow About Arbitrary Two-Dimensional Geometries," *AIAA Journal*, Vol. 16, No. 7, 1978, pp. 679–686.

[18]Steger, J. L., and Warming, R. F., "Flux Vector Splitting of the Inviscid Gasdynamic Equations with Applications to Finite-Difference Methods," *Journal of Computational Physics*, Vol. 40, No. 2, 1981, pp. 263–293.

[19]Hunt, B. L., and Dexter, P. C., "Pressures on a Slender Body at High Angle of Attack in a Very Low Turbulence Level Airstream," *High Angle of Attack Aerodynamics*, Paper 17, AGARD-CP-247, Oct. 1978.

[20]Dexter, P. C., and Hunt, B. L., "The Effects of Roll Angle on the Flow Over a Slender Body of Revolution at High Angle of Attack," AIAA Paper 81-0358, Jan. 1981.

[21]Schiff, L. B., Degani, D., and Gavali, S., "Numerical Simulation of Vortex Unsteadiness on Slender Bodies of Revolution at Large Incidence," AIAA Paper 89-0195, Jan. 1989.

[22]Levy, Y., Seginer, A., and Degani, D., "Graphical Representation of Three-Dimensional Vortical Flows by Means of Helicity Density and Normalized Helicity," AIAA Paper 88-2598, June 1988.

[23]Levy, Y., Degani, D., and Seginer, A., "Graphical Representation of Three-Dimensional Vortical Flows by Means of Helicity," *AIAA Journal*, Vol. 28, 1990, pp. 1347–1352.

[24]Moskovitz, C. A., Hall, R. M., and DeJarnette, F. R., "Effects of Nose Bluntness, Roughness and Surface Perturbations on the Asymmetric Flow Past Slender Bodies at Large Angles of Attack," AIAA Paper 88-2236CP, Aug. 1989.

[25]Zilliac, G. G., Degani, D., and Tobak, M., "Asymmetric Vortices on a Slender Body of Revolution," AIAA Paper 90-0389, Jan. 1990.

[26]Triantafyllou, G. S., Kupfer, K., and Bers, A., "Absolute Instabilities and Self-Sustained Oscillation in the Wakes of Circular Cylinder," *Physical Review Letters*, Vol. 59, No. 17, 1987, pp. 1014–1917.

[27]Chomaz, J. M., Huerre, P., and Redekopp, L. G., "Bifurcations to Local and Global Modes in Spatially Developing Flows," *Physical Review Letters*, Vol. 60, No. 1, 1988, pp. 25–28.

[28]Sreeninasan, K. R., Raghu, S., and Kyle, D., "Absolute Instabil-

ity in Variable Density Round Jets," *Experiments in Fluids*, Vol. 7, 1989, pp. 309–317.

[29]Yang, X., and Zebib, A., "Absolute and Convective Instability of a Cylinder Wake," *Physics of Fluids*, Vol. 1, No. 4, 1989, pp. 689–696.

[30]Wilkinson, S. P., and Malik, M. R., "Stability Experiments in the Flow over a Rotating Disk," *AIAA Journal*, Vol. 23, No. 4, 1985, pp. 588-595.

[31]Gaster, M., "The Role of Spatially Growing Waves in the Theory of Hydrodynamic Stability," *Progress in Aeronautical Sciences*, Vol. 6, edited by D. Kuchemann and L. H. G. Sterne, Pergamon, New York, 1965.

[32]Schubauer, G. B., and Skramstad, H. K., "Laminar Boundary Layer Oscillations and Transition on a Flat Plate," NACA Rept. 909, 1949.

[33]Moskovitz, C. A., DeJarnette, F. R., and Hall, R. M., "Experimental Investigation of a New Device to Control the Asymmetric Flowfield on Forebodies at Large Angles of Attack," AIAA Paper 90-0069, Jan. 1990.

[34]Degani, D., and Steger, J. L., "Comparison Between Navier-Stokes and Thin-Layer Computations for Separated Supersonic Flow," *AIAA Journal*, Vol. 21, No. 11, 1983, pp. 1604–1606.

[35]Degani, D., and Schiff, L. B., "Computation of Turbulent Supersonic Flows around Pointed Bodies Having Crossflow Separation," *Journal of Computational Physics*, Vol. 66, 1986, 173–196.

[36]Webster, W. P., and Shang, J. S., "Comparison Between Thin-Layer and Full Navier-Stokes Simulations Over a Supersonic Delta Wing," AIAA Paper 90-0589, Jan. 1990.